


Article

Nanoporous High-Entropy Alloy by Liquid Metal Dealloying

Artem Vladimirovich Okulov ¹, Soo-Hyun Joo ^{2,3}, Hyoung Seop Kim ⁴ , Hidemi Kato ²
and Ilya Vladimirovich Okulov ^{2,5,6,7,*}

¹ Division of Materials Mechanics, Institute of Materials Research, Helmholtz-Zentrum Geesthacht, 21502 Geesthacht, Germany; okulovtema@yandex.ru

² Institute for Materials Research, Tohoku University, Katahira 2-1-1, Sendai 980-8577, Japan; jjsh83@imr.tohoku.ac.jp (S.-H.J.); hikato@imr.tohoku.ac.jp (H.K.)

³ Department of Materials Science and Engineering, Dankook University, 119 Dandae-ro, Cheonan 31116, Korea

⁴ Department of Materials Science and Engineering Pohang, University of Science and Technology, 77 Cheongam-Ro, Pohang 37673, Korea; hskim@postech.ac.kr

⁵ Institute of Natural Sciences and Mathematics, Ural Federal University, 620000 Ekaterinburg, Russia

⁶ Faculty of Production Engineering, University of Bremen, Badgasteiner Str. 1, 28359 Bremen, Germany

⁷ Leibniz Institute for Materials Engineering-IWT, Badgasteiner Str. 3, 28359 Bremen, Germany

* Correspondence: okulovilya@yandex.ru; Tel.: +49-4212-185-1215

Received: 23 September 2020; Accepted: 15 October 2020; Published: 21 October 2020



Abstract: High-entropy nanomaterials possessing high accessible surface areas have demonstrated outstanding catalytic performance, beating that found for noble metals. In this communication, we report about the synthesis of a new, nanoporous, high-entropy alloy (HEA) possessing open porosity. The nanoporous, high-entropy Ta_{19.1}Mo_{20.5}Nb_{22.9}V₃₀Ni_{7.5} alloy (at%) was fabricated from a precursor (TaMoNbV)₂₅Ni₇₅ alloy (at%) by liquid metal dealloying using liquid magnesium (Mg). Directly after dealloying, the bicontinuous nanocomposite consisting of a Mg-rich phase and a phase with a bulk-centered cubic (bcc) structure was formed. The Mg-rich phase was removed with a 3M aqueous solution of nitric acid to obtain the open, porous, high-entropy Ta_{19.1}Mo_{20.5}Nb_{22.9}V₃₀Ni_{7.5} alloy (at%). The ligament size of this nanoporous HEA is about 69 ± 9 nm, indicating the high surface area in this material.

Keywords: high-entropy alloy; dealloying; liquid metal dealloying; nanoporous; catalysis

1. Introduction

High-entropy alloys (HEAs) have attracted intensive research during the past decade due to their unique properties [1–4]. Unlike the conventional alloy systems based on one principal element, or occasionally two principal elements, HEAs contain at least five major elements at concentrations ranging between 5 and 35 at%. The implicit hypothesis in the term “high-entropy” is that the high mixing entropy of these modern types of alloys can exceed the enthalpies of compound formation. Therefore, single-phase solid solutions are formed. The outstanding chemical and mechanical properties of HEAs [1,4–11] are directly related to the four “core effects”, i.e., high entropy, sluggish diffusion, severe lattice distortion, and the cocktail effect [12]. Especially, the sluggish diffusion effect is important for the exceptional high-temperature strength [13,14] and high-temperature structural stability of HEAs [13]. Recently, a number of HEA nanomaterials possessing high intrinsic catalytic activity for the decomposition of ammonia, CO oxidation, and water splitting were discovered [15–17]. In this case, the excellent functional, e.g., catalytic, properties can only be revealed for HEAs possessing a very large accessible surface area.

Several methods have been used for the synthesis of high-entropy nanomaterials possessing large surface areas, including chemical dealloying [17], sputtering [18], and carbothermal shock synthesis [4]. Recently, Joo et al. demonstrated the synthesis of nanoporous HEAs by liquid metal dealloying (LMD) [19]. Liquid metal dealloying, invented by Wada and Kato et al. in 2011 [20], is a metallurgical method for the synthesis of porous and nanocomposite materials [21–24]. In contrast to conventional chemical dealloying, the LMD method utilizes a metallic melt instead of a chemical etchant. Thus, during the LMD process, oxidation is prevented and reactive materials such as Mg [25] can be synthesized. To date, a wide variety of porous materials obtained by LMD have been reported, including silicon (Si) [26], steels [24,27–30], graphene (C) [31–34], chromium (Cr) [27], niobium (Nb) [35,36], titanium (Ti) [37,38], and titanium alloys (TiZr, TiHf, TiNb, TiFe, and TiMo) [23,38–41]. Moreover, LMD was successfully applied for the surface functionalization of biomedical Ti–6Al–4V and Ti–6Al–7Nb alloys [42,43], design of low modulus composites such as Fe–Mg [39,44], and synthesis of high-coercivity NdFeB-based permanent magnets [45]. Since the LMD process is typically conducted at elevated temperatures, it demonstrates significantly higher dealloying rates as compared to chemical dealloying. On the other hand, the drawback of LMD is a significant and unavoidable microstructural coarsening due to the high temperatures. The coarsening destroys the functional properties of the nanoporous materials associated with their high surface area. In our recent study, we demonstrated a material design principle enabling avoiding thermal coarsening in nanoporous materials [19]. In this communication, we report about the synthesis of a new, open, porous, high-entropy Ta_{19.1}Mo_{20.5}Nb_{22.9}V₃₀Ni_{7.5} (at%) alloy by the liquid metal dealloying of the (TaMoNbV)₂₅Ni₇₅ precursor alloy (at%).

2. Materials and Methods

The design of a material system for liquid metal dealloying begins from the selection of elements. The elements for the liquid metal dealloying are selected based on the enthalpy of mixture ($\Delta H_{(Mg-element)}^{mix}$) between a corrosive medium such as magnesium melt and the considered element (Figure 1a). Elements exhibiting a positive value of $\Delta H_{(Mg-element)}^{mix}$ such as Ti, V, Cr, Fe, Mn, Co, Zr, Nb, Mo, Hf, and Ta (Figure 1b) are immiscible in Mg and, therefore, self-organize into bicontinuous structures upon dealloying. At the same time, elements with a negative value of $\Delta H_{(Mg-element)}^{mix}$ such as B, Al, Si, P, Ca, Ni, Cu, Zn, Sr, Pd, Ag, In, Sn, Pt, and Au (Figure 1b) dissolve in Mg upon the dealloying process. Thereby, a large number of element combinations can be selected for liquid/solid metal dealloying and, particularly, for obtaining multicomponent porous scaffolds, including porous high-entropy alloys. To demonstrate the effectiveness of the above-described approach, a precursor (TaMoNbV)₂₅Ni₇₅ alloy (at%) was designed and dealloyed in magnesium at 1123 K for 20 min.

The precursor (TaMoNbV)₂₅Ni₇₅ alloy (at%) in the shape of rods (1 mm in diameter) was fabricated and prepared from pure metals (99.99%) with an arc melting device coupled with a suction casting set-up under an argon (Ar) atmosphere (Mini Arc Melter MAM-1, Edmund Bühler, Germany). To carry out dealloying, rods 2 mm long together with a magnesium mesh were heated in a glassy carbon crucible under Ar flow using an infrared furnace (IRF 10, Behr, Switzerland). Upon heating (at a heating rate of about 40 K s^{−1}), magnesium metal melts and diffuses into the precursor to selectively dissolve Ni out of the precursor alloy. The remaining elements diffuse along the metal/liquid interface [20,22] to form bicontinuous ligament structures. After dealloying, the crucible is cooled down to room temperature and the nanocomposite consisting of new phases, namely Mg-rich and high-entropy phases, is formed (Figure 2). To obtain porous HEA material, the Mg-rich phase was selectively etched out in 3 M HNO₃ for 5 h (Figure 2). Structural investigation of the precursor alloys and porous samples was performed by X-ray diffraction in Bragg–Brentano geometry (D8 Advance, Bruker, Germany) with Cu-K_α radiation. The device was equipped with a position-sensitive detector (LynxEye, Bruker, Germany), enabling us to achieve acceptable signal-to-noise ratios within a few hours of measuring time despite the smallness of the samples. Scanning electron microscopy (Nova Nanolab 200, FEI, Hillsboro, OR, USA) coupled with energy-dispersive X-ray analysis (EDAX, Weiterstadt, Germany) was used to explore the microstructure and composition.

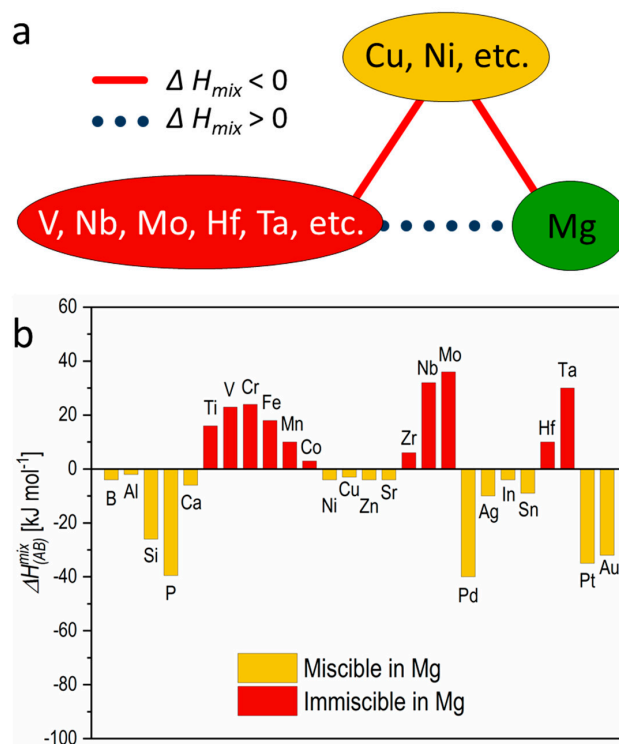


Figure 1. Selection of elements for liquid metal dealloying. (a) The values of $\Delta H_{(AB)}^{mix}$ (kJ/mol) calculated by Miedema's model for atomic pairs between Mg and elements indicated in the plot [46]; (b) Required relationship of the values of enthalpy of mixing between elements for the liquid metal dealloying of a master alloy AB in a liquid metal C.

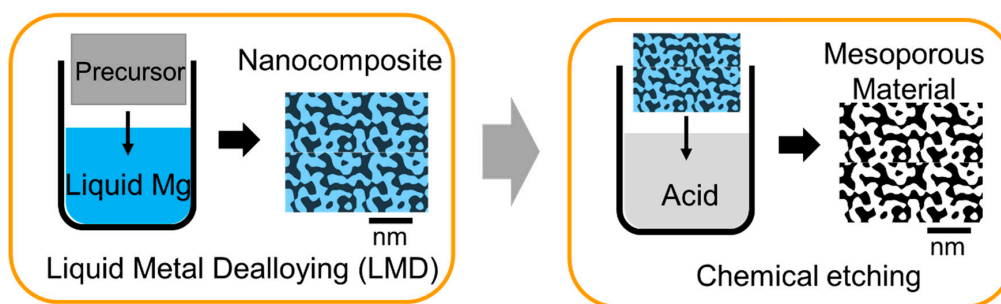


Figure 2. Schematic illustration of liquid metal dealloying process.

3. Results and Discussion

Figure 3 shows the X-ray diffraction pattern and microstructure of the final open nanoporous HEA. According to the X-ray analysis, the nanoporous HEA mainly consists of a phase with a bulk-centered cubic (bcc) structure and a minor amount of an unknown phase (Figure 3). According to the energy-dispersive X-ray analysis (EDX), the bcc phase is a solid solution of five elements with the following chemical composition: $\text{Ta}_{19.1}\text{Mo}_{20.5}\text{Nb}_{22.9}\text{V}_{30}\text{Ni}_{7.5}$ (at%). The single-phase structure and multicomponent chemical composition (the concentration of each element is above 5 at%) of the current porous material indicate that this is a high-entropy alloy. The SEM analysis reveals the nanoporous structure of the designed HEA (Figure 3). The average size of the ligaments is about 69 ± 9 nm, which is 1–2 orders of magnitude lower than is typically observed for the porous materials obtained by LMD [23,38]. The ligament coarsening during the liquid metal dealloying is primarily associated with surface diffusion [37]. Thus, the activation energy for the surface diffusion controls the coarsening. It seems that the sluggish diffusion effect observed in the high-entropy alloys [47]

prevents coarsening in the current nanoporous HEA. However, the controversial results regarding the sluggish diffusion phenomenon require a deeper understanding of the basic mechanisms suppressing coarsening in the nanoporous HEAs.

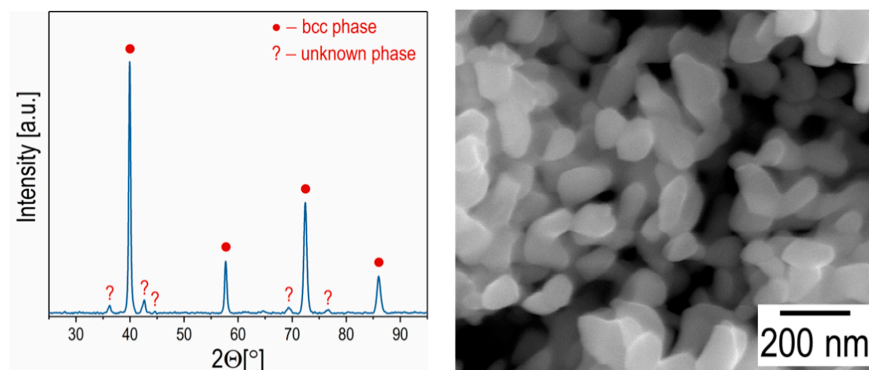


Figure 3. X-ray diffraction pattern and scanning electron micrograph of the nanoporous high-entropy TaMoNbVNi alloy.

As was proposed by Chen and Sieradzki [48], the microstructural length scale (ligament size) of porous materials fabricated by chemical dealloying at room temperature is correlated with the inverse “homologous dealloying temperature” or $1/T_H = T_{\text{melting point}}/T_{298\text{K}}$. This universal correlation was expanded by McCue et al. [49] to the porous materials obtained by liquid metal dealloying. It was shown that the porous materials obtained by LMD follow a similar trend. The homologous dealloying temperature, in this case, was modified to $T_H = T_{\text{melting point}}/T_{\text{dealloying temperature}}$. Later, Joo and Okulov et al. demonstrated that porous HEAs synthesized by LMD possess a different correlation of ligament size with homologous temperature [19]. Specifically, the universal relationship for the nanoporous HEAs shifts down by one order of magnitude towards the smaller-size regime. Similar to the reported nanoporous HEAs [19], the currently designed nanoporous HEA also deviates from the universal relationship proposed by Chen and Sieradzki [48] and validates the recent high-entropy design strategy [19] for suppressing thermal coarsening in nanoporous materials obtained by dealloying (Figure 4).

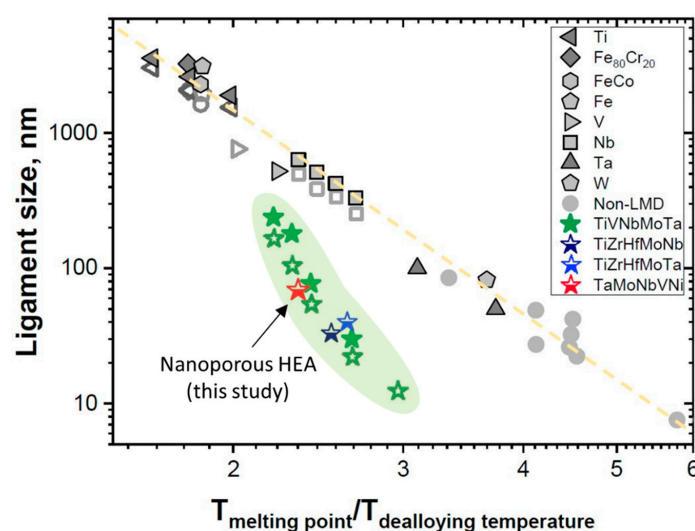


Figure 4. Ligament size versus homologous temperature in conventional nano- and microporous materials and the nanoporous high-entropy alloys (HEAs) [19] (note: non-LMD represents the nanoporous materials obtained by chemical dealloying [49]; the dealloying time is different from that for the LMD-based materials: 10 min—open symbols, 20 min—half-open symbols, and 60 min—closed symbols).

In summary, we have successfully designed a new, open, nanoporous, high-entropy Ta–Mo–Nb–V–Ni alloy by liquid metal dealloying based on the design strategy proposed in our recent study [19]. The currently developed open, porous HEA predominantly consists of a body-centered cubic (bcc) solid solution phase. The ligament size of the nanoporous Ta–Mo–Nb–V–Ni alloy after 20 min of dealloying at 1123 K is 69 ± 9 nm, which indicates its high stability against thermal coarsening. The nanoporous, high-entropy materials are promising candidates for functional applications such as catalysis.

Author Contributions: Conceptualization—H.K., H.S.K., and I.V.O.; formal analysis—A.V.O., S.-H.J., and I.V.O.; funding acquisition—H.K., H.S.K., and I.V.O.; investigation—A.V.O., S.-H.J., and I.V.O.; supervision—I.V.O., H.S.K., and H.K.; validation—A.V.O., I.V.O., and S.-H.J.; writing—original draft, A.V.O. and I.V.O.; writing—review and editing—all. All authors have read and agreed to the published version of the manuscript.

Funding: This research was funded by the International Collaboration Center, Institute for Materials Research (ICC-IMR), Tohoku University, Japan (no grant number) and the German Science Foundation under the Leibniz Program, grant number MA 3333/13-1.

Conflicts of Interest: The authors declare no conflict of interest.

References

1. Yeh, J. Recent Progress in High-entropy Alloys. *Ann. Chim. Sci. Mater.* **2006**, *31*, 633–648. [\[CrossRef\]](#)
2. Yeh, J.W.; Chen, S.K.; Lin, S.J.; Gan, J.Y.; Chin, T.S.; Shun, T.T.; Tsau, C.H.; Chang, S.Y. Nanostructured high-entropy alloys with multiple principal elements: Novel alloy design concepts and outcomes. *Adv. Eng. Mater.* **2004**, *6*, 299–303. [\[CrossRef\]](#)
3. Zhang, Y.; Zuo, T.T.; Tang, Z.; Gao, M.C.; Dahmen, K.A.; Liaw, P.K.; Lu, Z.P. Microstructures and properties of high-entropy alloys. *Prog. Mater. Sci.* **2014**, *61*, 1–93. [\[CrossRef\]](#)
4. Yao, Y.; Huang, Z.; Xie, P.; Lacey, S.D.; Jacob, R.J.; Xie, H.; Chen, F.; Nie, A.; Pu, T.; Rehwoldt, M.; et al. Carbothermal shock synthesis of high-entropy-alloy nanoparticles. *Science (80-.)* **2018**, *359*, 1489–1494. [\[CrossRef\]](#) [\[PubMed\]](#)
5. Gludovatz, B.; Hohenwarter, A.; Catoor, D.; Chang, E.H.; George, E.P.; Ritchie, R.O. A fracture-resistant high-entropy alloy for cryogenic applications. *Science (80-.)* **2014**, *345*, 1153–1158. [\[CrossRef\]](#) [\[PubMed\]](#)
6. Senkov, O.N.; Wilks, G.B.; Miracle, D.B.; Chuang, C.P.; Liaw, P.K. Refractory high-entropy alloys. *Intermetallics* **2010**, *18*, 1758–1765. [\[CrossRef\]](#)
7. Senkov, O.N.; Scott, J.M.; Senkova, S.V.; Miracle, D.B.; Woodward, C.F. Microstructure and room temperature properties of a high-entropy TaNbHfZrTi alloy. *J. Alloys Compd.* **2011**, *509*, 6043–6048. [\[CrossRef\]](#)
8. Okulov, I.V.; Wendrock, H.; Volegov, A.S.; Attar, H.; Kühn, U.; Skrotzki, W.; Eckert, J. High strength beta titanium alloys: New design approach. *Mater. Sci. Eng. A* **2015**, *628*, 297–302. [\[CrossRef\]](#)
9. Okulov, I.V.; Bönnisch, M.; Okulov, A.V.; Volegov, A.S.; Attar, H.; Ehtemam-Haghighi, S.; Calin, M.; Wang, Z.; Hohenwarter, A.; Kaban, I.; et al. Phase formation, microstructure and deformation behavior of heavily alloyed TiNb- and TiV-based titanium alloys. *Mater. Sci. Eng. A* **2018**, *733*, 80–86. [\[CrossRef\]](#)
10. Tsai, M.H.; Yeh, J.W.; Gan, J.Y. Diffusion barrier properties of AlMoNbSiTaTiVZr high-entropy alloy layer between copper and silicon. *Thin Solid Films* **2008**, *516*, 5527–5530. [\[CrossRef\]](#)
11. Li, Z.; Pradeep, K.G.; Deng, Y.; Raabe, D.; Tasan, C.C. Metastable high-entropy dual-phase alloys overcome the strength–ductility trade-off. *Nature* **2016**, *534*, 227–230. [\[CrossRef\]](#) [\[PubMed\]](#)
12. Yeh, J.W. Physical Metallurgy of High-Entropy Alloys. *J. Miner. Met. Mater. Soc.* **2015**, *67*, 2254–2261. [\[CrossRef\]](#)
13. Senkov, O.N.; Wilks, G.B.; Scott, J.M.; Miracle, D.B. Mechanical properties of Nb₂₅Mo₂₅Ta₂₅W₂₅ and V₂₀Nb₂₀Mo₂₀Ta₂₀W₂₀. *Intermetallics* **2011**, *19*, 698–706. [\[CrossRef\]](#)
14. Senkov, O.N.; Senkova, S.V.; Woodward, C. Effect of aluminum on the microstructure and properties of two refractory high-entropy alloys. *Acta Mater.* **2014**, *68*, 214–228. [\[CrossRef\]](#)
15. Xie, P.; Yao, Y.; Huang, Z.; Liu, Z.; Zhang, J.; Li, T.; Wang, G.; Shahbazian-Yassar, R.; Hu, L.; Wang, C. Highly efficient decomposition of ammonia using high-entropy alloy catalysts. *Nat. Commun.* **2019**, *10*, 1–12. [\[CrossRef\]](#)
16. Qiu, H.J.; Fang, G.; Wen, Y.; Liu, P.; Xie, G.; Liu, X.; Sun, S. Nanoporous high-entropy alloys for highly stable and efficient catalysts. *J. Mater. Chem. A* **2019**, *7*, 6499–6506. [\[CrossRef\]](#)

17. Jin, Z.; Lv, J.; Jia, H.; Liu, W.; Li, H.; Chen, Z.; Lin, X.; Xie, G.; Liu, X.; Sun, S.; et al. Nanoporous Al-Ni-Co-Ir-Mo High-Entropy Alloy for Record-High Water Splitting Activity in Acidic Environments. *Small* **2019**, *15*, 1–7. [[CrossRef](#)]
18. Löffler, T.; Meyer, H.; Savan, A.; Wilde, P.; Garzón Manjón, A.; Chen, Y.T.; Ventosa, E.; Scheu, C.; Ludwig, A.; Schuhmann, W. Discovery of a Multinary Noble Metal-Free Oxygen Reduction Catalyst. *Adv. Energy Mater.* **2018**, *8*, 1–7. [[CrossRef](#)]
19. Joo, S.-H.; Bae, J.W.; Park, W.-Y.; Shimada, Y.; Wada, T.; Kim, H.S.; Takeuchi, A.; Konno, T.J.; Kato, H.; Okulov, I.V. Beating Thermal Coarsening in Nanoporous Materials via High-Entropy Design. *Adv. Mater.* **2020**, *32*, 1906160. [[CrossRef](#)]
20. Wada, T.; Yubuta, K.; Inoue, A.; Kato, H. Dealloying by metallic melt. *Mater. Lett.* **2011**, *65*, 1076–1078. [[CrossRef](#)]
21. McCue, I.; Gaskey, B.; Geslin, P.A.; Karma, A.; Erlebacher, J. Kinetics and morphological evolution of liquid metal dealloying. *Acta Mater.* **2016**, *115*, 10–23. [[CrossRef](#)]
22. Geslin, P.; Mccue, I.; Erlebacher, J.; Karma, A. Topology-generating interfacial pattern formation during liquid metal dealloying. *Nat. Commun.* **2015**, *6*, 1–19. [[CrossRef](#)] [[PubMed](#)]
23. Okulov, I.V.; Okulov, A.V.; Soldatov, I.V.; Luthringer, B.; Willumeit-Römer, R.; Wada, T.; Kato, H.; Weissmüller, J.; Markmann, J. Open porous dealloying-based biomaterials as a novel biomaterial platform. *Mater. Sci. Eng. C* **2018**, *83*, 95–103. [[CrossRef](#)] [[PubMed](#)]
24. Joo, S.-H.; Kato, H. Transformation mechanisms and governing orientation relationships through selective dissolution of Ni via liquid metal dealloying from (FeCo)_xNi_{100-x} precursors. *Mater. Des.* **2020**, *185*, 108271. [[CrossRef](#)]
25. Okulov, I.V.; Lamaka, S.V.; Wada, T.; Yubuta, K.; Zheludkevich, M.L.; Weissmüller, J.; Markmann, J.; Kato, H. Nanoporous magnesium. *Nano Res.* **2018**, *11*, 6428–6435. [[CrossRef](#)]
26. Wada, T.; Ichitsubo, T.; Yubuta, K.; Segawa, H.; Yoshida, H.; Kato, H. Bulk-nanoporous-silicon negative electrode with extremely high cyclability for lithium-ion batteries prepared using a top-down process. *Nano Lett.* **2014**, *14*, 4505–4510. [[CrossRef](#)]
27. Wada, T.; Kato, H. Three-dimensional open-cell macroporous iron, chromium and ferritic stainless steel. *Scr. Mater.* **2013**, *68*, 723–726. [[CrossRef](#)]
28. Joo, S.-H.; Wada, T.; Kato, H. Development of porous FeCo by liquid metal dealloying: Evolution of porous morphology and effect of interaction between ligaments and melt. *Mater. Des.* **2019**, *180*, 107908. [[CrossRef](#)]
29. Mokhtari, M.; Wada, T.; Le Burlot, C.; Mary, N.; Duchet-Rumeau, J.; Kato, H.; Maire, E. Low cost high specific surface architected nanoporous metal with corrosion resistance produced by liquid metal dealloying from commercial nickel superalloy. *Scr. Mater.* **2019**, *163*, 5–8. [[CrossRef](#)]
30. Mokhtari, M.; Wada, T.; Le Burlot, C.; Duchet-Rumeau, J.; Kato, H.; Maire, E.; Mary, N. Corrosion resistance of porous ferritic stainless steel produced by liquid metal dealloying of Incoloy 800. *Corros. Sci.* **2020**, 108468. [[CrossRef](#)]
31. Yu, S.G.; Yubuta, K.; Wada, T.; Kato, H. Three-dimensional bicontinuous porous graphite generated in low temperature metallic liquid. *Carbon N. Y.* **2016**, *96*, 403–410. [[CrossRef](#)]
32. Greenidge, G.; Erlebacher, J. Porous graphite fabricated by liquid metal dealloying of silicon carbide. *Carbon N. Y.* **2020**, *165*, 45–54. [[CrossRef](#)]
33. Park, W.-Y.; Wada, T.; Joo, S.-H.; Han, J.; Kato, H. Novel hierarchical nanoporous graphene nanoplatelets with excellent rate capabilities produced via self-templating liquid metal dealloying. *Mater. Today Commun.* **2020**, *24*, 101120. [[CrossRef](#)]
34. Shao, J.-C.; Jin, H.-J. From liquid metal dealloying to liquid metal expulsion. *J. Mater. Sci.* **2020**, *55*, 8337–8345. [[CrossRef](#)]
35. Kim, J.W.; Tsuda, M.; Wada, T.; Yubuta, K.; Kim, S.G.; Kato, H. Optimizing niobium dealloying with metallic melt to fabricate porous structure for electrolytic capacitors. *Acta Mater.* **2015**, *84*, 497–505. [[CrossRef](#)]
36. Kim, J.W.; Wada, T.; Kim, S.G.; Kato, H. Sub-micron porous niobium solid electrolytic capacitor prepared by dealloying in a metallic melt. *Mater. Lett.* **2014**, *116*, 223–226. [[CrossRef](#)]
37. Tsuda, M.; Wada, T.; Kato, H. Kinetics of formation and coarsening of nanoporous α -titanium dealloyed with Mg melt. *J. Appl. Phys.* **2013**, *114*. [[CrossRef](#)]
38. Okulov, I.V.; Weissmüller, J.; Markmann, J. Dealloying-based interpenetrating-phase nanocomposites matching the elastic behavior of human bone. *Sci. Rep.* **2017**, *7*, 20. [[CrossRef](#)]

39. Okulov, A.V.; Volegov, A.S.; Weissmüller, J.; Markmann, J.; Okulov, I.V. Dealloying-based metal-polymer composites for biomedical applications. *Scr. Mater.* **2018**, *146*, 290–294. [[CrossRef](#)]
40. Okulov, I.V.; Okulov, A.V.; Volegov, A.S.; Markmann, J. Tuning microstructure and mechanical properties of open porous TiNb and TiFe alloys by optimization of dealloying parameters. *Scr. Mater.* **2018**, *154*, 68–72. [[CrossRef](#)]
41. Berger, S.A.; Okulov, I.V. Open porous $\alpha + \beta$ titanium alloy by liquid metal dealloying for biomedical applications. *Metals* **2020**, in press.
42. Okulov, I.V.; Joo, S.-H.; Okulov, A.V.; Volegov, A.S.; Luthringer, B.; Willumeit-Römer, R.; Zhang, L.; Mädler, L.; Eckert, J.; Kato, H. Surface Functionalization of Biomedical Ti-6Al-7Nb Alloy by Liquid Metal Dealloying. *Nanomaterials* **2020**, *10*. [[CrossRef](#)]
43. Fukuzumi, Y.; Wada, T.; Kato, H. *Surface Improvement for Biocompatibility of Ti-6Al-4V by Dealloying in Metallic Melt BT-Interface Oral Health Science 2014*; Sasaki, K., Suzuki, O., Takahashi, N., Eds.; Springer: Tokyo, Japan, 2015; pp. 93–101.
44. Okulov, I.V.; Geslin, P.-A.; Soldatov, I.V.; Ovri, H.; Joo, S.-H.; Kato, H. Anomalously low modulus of the interpenetrating-phase composite of Fe and Mg obtained by liquid metal dealloying. *Scr. Mater.* **2019**, *163*, 133–136. [[CrossRef](#)]
45. Volegov, A.S.; Andreev, S.V.; Selezneva, N.V.; Ryzhikhin, I.A.; Kudrevatykh, N.V.; Mädler, L.; Okulov, I.V. Additive manufacturing of heavy rare earth free high-coercivity permanent magnets. *Acta Mater.* **2020**, *188*, 733–739. [[CrossRef](#)]
46. Takeuchi, A.; Inoue, A. Metallic Glasses By Atomic Size Difference, Heat of Mixing and Period of Constituent Elements and Its Application To Characterization of the Main Alloying Element. *Mater. Trans.* **2005**, *46*, 2817–2829. [[CrossRef](#)]
47. Tsai, K.Y.; Tsai, M.H.; Yeh, J.W. Sluggish diffusion in Co-Cr-Fe-Mn-Ni high-entropy alloys. *Acta Mater.* **2013**, *61*, 4887–4897. [[CrossRef](#)]
48. Chen, Q.; Sieradzki, K. Spontaneous evolution of bicontinuous nanostructures in dealloyed Li-based systems. *Nat. Mater.* **2013**, *12*, 1102–1106. [[CrossRef](#)]
49. McCue, I.; Karma, A.; Erlebacher, J. Pattern formation during electrochemical and liquid metal dealloying. *MRS Bull.* **2018**, *43*, 27–34. [[CrossRef](#)]

Publisher's Note: MDPI stays neutral with regard to jurisdictional claims in published maps and institutional affiliations.



© 2020 by the authors. Licensee MDPI, Basel, Switzerland. This article is an open access article distributed under the terms and conditions of the Creative Commons Attribution (CC BY) license (<http://creativecommons.org/licenses/by/4.0/>).